


[nature](#) > [nature medicine](#) > [articles](#) > [article](#)

Article | [Published: 19 February 2024](#)

A terminal metabolite of niacin promotes vascular inflammation and contributes to cardiovascular disease risk

[Marc Ferrell](#), [Zeneng Wang](#), [James T. Anderson](#), [Xinmin S. Li](#), [Marco Witkowski](#), [Joseph A. DiDonato](#), [James R. Hilser](#), [Jaana A. Hartiala](#), [Arash Haghikia](#), [Tomas Cajka](#), [Oliver Fiehn](#), [Naseer Sangwan](#), [Ilja Demuth](#), [Maximilian König](#), [Elisabeth Steinhagen-Thiessen](#), [Ulf Landmesser](#), [W. H. Wilson Tang](#), [Hooman Allayee](#) & [Stanley L. Hazen](#) 

Nature Medicine **30**, 424–434 (2024)

6287 Accesses | 1501 Altmetric | [Metrics](#)

Abstract

Despite intensive preventive cardiovascular disease (CVD) efforts, substantial residual CVD risk remains even for individuals receiving all guideline-recommended interventions. Niacin is an essential micronutrient fortified in food staples, but its role in CVD is not well understood. In this study, untargeted metabolomics analysis of fasting plasma from stable cardiac patients in a prospective discovery cohort ($n = 1,162$ total, $n = 422$ females) suggested that niacin metabolism was associated with incident major adverse cardiovascular events (MACE). Serum levels of the terminal metabolites of excess niacin, N1-methyl-2-pyridone-5-carboxamide (2PY) and N1-methyl-4-pyridone-3-carboxamide (4PY), were associated with increased 3-year MACE risk in two validation cohorts (US $n = 2,331$ total, $n = 774$ females; European $n = 832$ total, $n = 249$ females) (adjusted hazard ratio (HR) (95% confidence interval) for 2PY: 1.64 (1.10–2.42) and 2.02 (1.29–3.18), respectively; for 4PY: 1.89 (1.26–2.84) and 1.99 (1.26–3.14), respectively). Phenome-wide association analysis of the genetic variant rs10496731, which was significantly associated with both 2PY and 4PY levels, revealed an association of this

variant with levels of soluble vascular adhesion molecule 1 (sVCAM-1). Further meta-analysis confirmed association of rs10496731 with sVCAM-1 ($n = 106,000$ total, $n = 53,075$ females, $P = 3.6 \times 10^{-18}$). Moreover, sVCAM-1 levels were significantly correlated with both 2PY and 4PY in a validation cohort ($n = 974$ total, $n = 333$ females) (2PY: $\rho = 0.13$, $P = 7.7 \times 10^{-5}$; 4PY: $\rho = 0.18$, $P = 1.1 \times 10^{-8}$). Lastly, treatment with physiological levels of 4PY, but not its structural isomer 2PY, induced expression of VCAM-1 and leukocyte adherence to vascular endothelium in mice. Collectively, these results indicate that the terminal breakdown products of excess niacin, 2PY and 4PY, are both associated with residual CVD risk. They also suggest an inflammation-dependent mechanism underlying the clinical association between 4PY and MACE.

This is a preview of subscription content, [access via your institution](#)

Access options

Access Nature and 54 other Nature Portfolio journals

Get Nature+, our best-value online-access subscription

\$29.99 / 30 days

cancel any time

[Learn more](#)

**Rent or buy this
article**

Prices vary by article type

Subscribe to this journal

Receive 12 print issues and online access

from \$1.95

\$209.00 per year

to \$39.95

only \$17.42 per issue

[Learn more](#)[Learn more](#)

Prices may be subject to local taxes which are calculated during checkout

Additional access options:

- [Log in](#)
- [Learn about institutional subscriptions](#)
- [Read our FAQs](#)
- [Contact customer support](#)

Data availability

Source data for figures and tables included in this paper were deposited to the *Nature Medicine* website as Source Data. The DNA sequences and sequence maps of AAVs used are available at <https://doi.org/10.5281/zenodo.8357441>. Summary statistics for the meta-analyses for 2PY and 4PY are also available at <https://doi.org/10.5281/zenodo.8357441>. There are restrictions on the availability of some of the clinical data generated in the present study for the US and EU validation cohorts because the informed consent from participants in these studies does not permit sharing data outside each respective institution without authorization. Where permissible, the datasets generated and/or analyzed during the present studies are available from the corresponding author, S.L.H. (hazens@ccf.org), upon reasonable request. Individual-level data used in the present study are available upon application to

the UK Biobank (<https://www.ukbiobank.ac.uk/>). [Source data](#) are provided with this paper.

Code availability

Custom code is available at <https://doi.org/10.5281/zenodo.8357441>.

References

1. Virani, S. S. et al. Heart Disease and Stroke Statistics—2023 update: a report from the American Heart Association. *Circulation* **147**, 1772–1782 (2023).
 2. D’Agostino, R. B. et al. General cardiovascular risk profile for use in primary care: the Framingham Heart Study. *Circulation* **117**, 743–753 (2008).
 3. Ridker, P. M. et al. Cardiovascular efficacy and safety of bococizumab in high-risk patients. *N. Engl. J. Med.* **376**, 1527–1539 (2017).
 4. Sabatine, M. S. et al. Evolocumab and clinical outcomes in patients with cardiovascular disease. *N. Engl. J. Med.* **376**, 1713–1722 (2017).
 5. Pradhan, A. D., Aday, A. W., Rose, L. M. & Ridker, P. M. Residual inflammatory risk on treatment with PCSK9 inhibition and statin therapy. *Circulation* **138**, 141–149 (2018).
 6. Bohula, E. A. et al. Inflammatory and cholesterol risk in the FOURIER trial. *Circulation* **138**, 131–140 (2018).
-

7. Makarov, M. V., Trammell, S. A. J. & Migaud, M. E. The chemistry of the vitamin B3 metabolome. *Biochem. Soc. Trans.* **47**, 131–147 (2019).

8. Wan, P., Moat, S. & Anstey, A. Pellagra: a review with emphasis on photosensitivity. *Br. J. Dermatol.* **164**, 1188–1200 (2011).

9. *Dietary Reference Intakes: The Essential Guide to Nutrient Requirements* (eds Otten, J. J., Hellwig, J. P. & Meyers, L. D) (The National Academies Press, 2006).

10. Stierman, B. et al. National Health and Nutrition Examination Survey 2017–March 2020 Prepandemic Data Files—Development of Files and Prevalence Estimates for Selected Health Outcomes. *National Health Statistics Reports* **158**, <https://doi.org/10.15620/cdc:106273> (2021).

11. Stamler, J. The Coronary Drug Project—findings with regard to estrogen, dextrothyroxine, clofibrate and niacin. *Adv. Exp. Med. Biol.* **82**, 52–75 (1977).

12. Landmesser, U. The difficult search for a ‘partner’ of statins in lipid-targeted prevention of vascular events: the re-emergence and fall of niacin. *Eur. Heart J.* **34**, 1254–1257 (2013).

13. Lloyd-Jones, D. M. Niacin and HDL cholesterol—time to face facts. *N. Engl. J. Med.* **371**, 271–273 (2014).

14. Landray, M. J., Haynes, R. & Hopewell, J. C. Effects of extended-release niacin with laropiprant in high-risk patients. *N. Engl. J. Med.* **371**, 203–212 (2014).

15. Boden, W. et al. Niacin in patients with low HDL cholesterol levels receiving intensive statin therapy. *N. Engl. J. Med.* **365**, 2255–2267 (2011).

16. Jenkins, D. J. A. et al. Supplemental vitamins and minerals for CVD prevention and treatment. *J. Am. Coll. Cardiol.* **71**, 2570–2584 (2018).

17. Li, X. S. et al. Untargeted metabolomics identifies trimethyllysine, a TMAO-producing nutrient precursor, as a predictor of incident cardiovascular disease risk. *JCI Insight* **3**, e99096 (2018).

18. Wang, Z. et al. Gut flora metabolism of phosphatidylcholine promotes cardiovascular disease. *Nature* **472**, 57–65 (2011).

19. Nemet, I. et al. A cardiovascular disease-linked gut microbial metabolite acts via adrenergic receptors. *Cell* **180**, 862–877 (2020).

20. Witkowski, M. et al. The artificial sweetener erythritol and cardiovascular event risk. *Nat. Med.* **29**, 710–718 (2023).

21. Abelson, D., Boyle, A. & Seligson, H. Identification of N'-methyl-4-pyridone-3-carboxamide in human plasma. *J. Biol. Chem.* **238**, 717–718 (1962).

22. Menon, R. et al. Effect of the rate of niacin administration on the plasma and urine pharmacokinetics of niacin and its metabolites. *J. Clin. Pharm.* **47**, 681–688 (2007).

23. GTEx Consortium. The Genotype-Tissue Expression (GTEx) project. *Nat. Genet.* **45**, 580–585 (2013).

24. Sun, B. et al. Genomic atlas of the human plasma proteome. *Nature* **558**, 73–79 (2018).

25. Gudjonsson, G. et al. A genome-wide association study of serum proteins reveals shared loci with common diseases. *Nat. Comm.* **13**, 480 (2022).

26. Dansky, H. M. et al. Adhesion of monocytes to arterial endothelium and initiation of atherosclerosis are critically dependent on vascular cell adhesion molecule-1 gene dosage. *Arterioscler. Thromb. Vasc. Biol.* **21**, 1662–1667 (2001).

27. Cybulsky, M. I. et al. A major role for VCAM-1, but not ICAM-1, in early atherosclerosis. *J. Clin. Invest.* **107**, 1255–1262 (2001).

28. Sun, B. et al. Plasma proteomic associations with genetics and health in the UK Biobank. *Nature* **622**, 329–338 (2023).

29. Aragam, K. et al. Discovery and systematic characterization of risk variants and genes for coronary artery disease in over a million participants. *Nat. Genet.* **54**, 1803–1815 (2022).

30. Hartiala, J. et al. Genome-wide analysis identifies novel susceptibility loci for myocardial infarction. *Eur. Heart J.* **42**, 919–933 (2021).

31. Mishra, A. et al. Stroke genetics informs drug discovery and risk prediction across ancestries. *Nature* **611**, 115–123 (2022).

32. Chen, F. et al. Association among dietary supplement use, nutrient intake, and mortality among U.S. adults. *Ann. Intern. Med.* **170**, 604–613 (2019).

33. Tyler, J. et al. Global concerns with B vitamin statuses: biofortification, fortification, hidden hunger, interactions, and toxicity. *Compr. Rev. Food Sci. Food Saf.* **18**, 1968–1964 (2019).

34. Visseren, F. L. J. et al. 2021 ESC Guidelines on cardiovascular disease prevention in clinical practice. *Eur. Heart J.* **42**, 3227–3337 (2021).

35. Mangione, C. M. et al. Vitamin, mineral, and multivitamin supplementation to prevent cardiovascular disease and cancer: US Preventive Services Task Force recommendation statement. *JAMA* **327**, 2326–2333 (2022).

36. Grundy, S. M. et al. 2018
AHA/ACC/AACVPR/AAPA/ABC/ACPM/ADA/AGS/APHA/ASPC/NLA/PCNA guideline on the management of blood cholesterol: a report of the American College of Cardiology/American Heart Association Task Force on Clinical Practice Guidelines. *J. Am. Coll. Cardiol.* **73**, e285–e350 (2019).

37. Teo, K. K. et al. Extended-release niacin therapy and risk of ischemic stroke in patients with cardiovascular disease the atherothrombosis intervention in metabolic syndrome with low HDL/high triglycerides: impact on global health outcome (AIM-HIGH) trial. *Stroke* **44**, 2688–2693 (2013).

38. US Department of Agriculture Food Data Central. <https://fdc.nal.usda.gov/>

39. US Department of Agriculture Center for Nutrition Policy and Promotion. <https://www.fns.usda.gov/cnpp>

40. Elhassan, Y. S. et al. Nicotinamide riboside augments the aged human skeletal muscle NAD⁺ metabolome and induces article nicotinamide riboside augments the aged human skeletal muscle NAD⁺ metabolome and induces transcriptomic and anti-inflammatory signatures. *Cell Rep.* **28**, 1717–1728 (2019).

41. Trammell, S. A. J. et al. Nicotinamide riboside is uniquely and orally bioavailable in mice and humans. *Nat. Commun.* **7**, 12948 (2016).

42. Yoshino, M., Yohino, J., Kayser, B., Imai, S.-I. & Klein, S. Nicotinamide mononucleotide increases muscle insulin sensitivity in prediabetic women. *Science* **373**, 1224–1229 (2021).

43. Yi, L. et al. The efficacy and safety of β -nicotinamide mononucleotide (NMN) supplementation in healthy middle-aged adults: a randomized, multicenter, double-blind, placebo-controlled, parallel-group, dose-dependent clinical trial. *Geroscience* **45**, 29–43 (2022).

44. Chini, E. Effects of vitamin B3 derivative nicotinamide riboside (NR) in bone, skeletal muscle and metabolic functions in aging. [NCT03818802](#)

45. Slow age: interventions to slow aging in humans. [NCT05593939](#)

46. The effect of NAD supplementation on brain vascular health in aging. [NCT05483465](#)

47. Martens, C. R. et al. Chronic nicotinamide riboside supplementation is well-tolerated and elevates NAD⁺ in healthy middle-aged and older adults. *Nat. Commun.* **9**, 1286 (2018).

48. Cantó, C., Menzies, K. J. & Auwerx, J. NAD⁺ metabolism and the control of energy homeostasis: a balancing act between mitochondria and the nucleus. *Cell Metab.* **22**, 31–53 (2015).

49. Lenglet, A. et al. N-methyl-2-pyridone-5-carboxamide (2PY)—major metabolite of nicotinamide: an update on an old uremic toxin. *Toxins (Basel)* **8**, 339 (2016).

50. Horwitt, M., Harper, A. & Henderson, L. Niacin–tryptophan relationships for evaluating niacin equivalents. *Am. J. Clin. Nutr.* **34**, 423–427 (1981).

51. Pellicciari, R. et al. α -Amino- β -carboxymuconate- ϵ -semialdehyde decarboxylase (ACMSD) inhibitors as novel modulators of de novo nicotinamide adenine dinucleotide (NAD⁺) biosynthesis. *J. Med. Chem.* **61**, 745–759 (2018).

52. Katsyuba, E. et al. De novo NAD⁺ synthesis enhances mitochondrial function and improves health. *Nature* **563**, 354–359 (2018).
-
53. Yin, X. et al. Genome-wide association studies of metabolites in Finnish men identify disease-relevant loci. *Nat. Comm.* **13**, 1664 (2022).
-
54. Hemani, G. et al. The MR-Base platform supports systematic causal inference across the human phenome. *eLife*. **7**, e34408 (2018).
-
55. Ridker, P. M. et al. Antiinflammatory therapy with canakinumab for atherosclerotic disease. *N. Engl. J. Med.* **377**, 1119–1131 (2017).
-
56. Ley, K., Laudanna, C., Cybulsky, M. I. & Nourshargh, S. Getting to the site of inflammation: the leukocyte adhesion cascade updated. *Nat. Rev. Immunol.* **7**, 678–689 (2007).
-
57. Libby, P. Inflammation during the life cycle of the atherosclerotic plaque. *Cardiovasc. Res.* **117**, 2525–2536 (2021).
-
58. Marui, N. et al. Vascular cell adhesion molecule-1 (VCAM-1) gene transcription and expression are regulated through an antioxidant-sensitive mechanism in human vascular endothelial cells. *J. Clin. Invest.* **92**, 1866–1874 (1993).
-
59. Pigott, R., Dillon, L. P., Hemingway, I. H. & Gearing, A. J. H. Soluble forms of E-selectin, ICAM-1 and VCAM-1 are present in the supernatants of cytokine activated cultured endothelial cells. *Biochem. Biophys. Res. Commun.* **187**, 584–589 (1992).
-

60. Blankenberg, S. et al. Circulating cell adhesion molecules and death in patients with coronary artery disease. *Circulation* **104**, 1336–1342 (2001).

61. Koeth, R. A. et al. Intestinal microbiota metabolism of L-carnitine, a nutrient in red meat, promotes atherosclerosis. *Nat. Med.* **19**, 576–585 (2013).

62. Brennan, M. L. et al. Comprehensive peroxidase-based hematologic profiling for the prediction of 1-year myocardial infarction and death. *Circulation* **122**, 70–79 (2010).

63. König, M. et al. Cohort profile: role of lipoproteins in cardiovascular disease—the LipidCardio study. *BMJ Open* **9**, e030097 (2019).

64. Inker, L. A. et al. New creatinine- and cystatin C–based equations to estimate GFR without race. *N. Engl. J. Med.* **385**, 1737–1749 (2021).

65. STROBE statement—checklist of items that should be included in reports of observational studies (STROBE initiative). *Int. J. Public Health* **53**, 3–4 (2008).

66. Pluskal, T., Castillo, S., Villar-Briones, A. & Orešič, M. MZmine 2: modular framework for processing, visualizing, and analyzing mass spectrometry-based molecular profile data. *BMC Bioinformatics* **11**, 395 (2010).

67. Li, S. et al. Predicting network activity from high throughput metabolomics. *PLoS Comput. Biol.* **9**, e1003123 (2013).

68. Chong, J. et al. MetaboAnalyst 4.0: towards more transparent and integrative metabolomics analysis. *Nucleic Acids Res.* **46**, W486–W494 (2018).
-
69. Magnusson, M. et al. A diabetes-predictive amino acid score and future cardiovascular disease. *Eur. Heart J.* **34**, 1982–1989 (2013).
-
70. Du, X. et al. Relationships between circulating branched chain amino acid concentrations and risk of adverse cardiovascular events in patients with STEMI treated with PCI. *Sci. Rep.* **8**, 6–13 (2018).
-
71. Soda, K., Kano, Y. & Chiba, F. Food polyamine and cardiovascular disease—an epidemiological study. *Glob. J. Health Sci.* **4**, 170–178 (2012).
-
72. Lang, R. et al. Development of a hydrophilic liquid interaction chromatography–high-performance liquid chromatography–tandem mass spectrometry based stable isotope dilution analysis and pharmacokinetic studies on bioactive pyridines in human plasma and urine after coffee. *Anal. Chem.* **82**, 1486–1497 (2010).
-
73. Ruf, S. et al. Novel nicotinamide analog as inhibitor of nicotinamide N-methyltransferase. *Bioorg. Med. Chem. Lett.* **28**, 922–925 (2018).
-
74. Chang, C. C. et al. Second-generation PLINK: rising to the challenge of larger and richer datasets. *Gigascience* **4**, 7 (2015).
-
75. Willer, C. J., Li, Y. & Abecasis, G. R. METAL: fast and efficient meta-analysis of genomewide association scans. *Bioinformatics* **26**, 2190–2191 (2010).
-

76. Begum, F., Ghosh, D., Tseng, G. C. & Feingold, E. Comprehensive literature review and statistical considerations for GWAS meta-analysis. *Nucleic Acids Res.* **40**, 3777–3784 (2012).
-
77. Pucci, L. et al. Tissue expression and biochemical characterization of human 2-amino 3-carboxymuconate 6-semialdehyde decarboxylase, a key enzyme in tryptophan catabolism. *FEBS* **274**, 827–840 (2007).
-
78. Bycroft, C. et al. The UK Biobank resource with deep phenotyping and genomic data. *Nature* **561**, 203–209 (2018).
-
79. Burgess, S. Sample size and power calculations in Mendelian randomization with a single instrumental variable and a binary outcome. *Int J. Epidemiol.* **43**, 922–929 (2014).
-
80. Ram, S. et al. Pixelwise H-score: a novel digital image analysis-based metric to quantify membrane biomarker expression from immunohistochemistry images. *PLoS ONE* **16**, e0245638 (2021).
-
81. Xiao, W. et al. Immunometabolic endothelial phenotypes: integrating inflammation and glucose metabolism. *Circ. Res.* **129**, 9–29 (2021).
-
82. Bolger, A. et al. Trimmomatic: a flexible trimmer for Illumina sequence data. *Bioinformatics* **30**, 2114–2120 (2014).
-

83. Dobin, A. et al. STAR: ultrafast universal RNA-seq aligner. *Bioinformatics* **29**, 15–21 (2013).

84. Robinson, M. et al. edgeR: a Bioconductor package for differential expression analysis of digital gene expression data. *Bioinformatics* **26**, 139–140 (2010).

85. Alexa, A. & Rahnenfuhrer, J. topGO: enrichment analysis for Gene Ontology. Bioconductor. <https://doi.org/10.18129/B9.bioc.topGO> (2023).

Acknowledgements

This work was supported by grants from the National Institutes of Health (NIH) (both the National Heart, Lung, and Blood Institute and the Office of Dietary Supplements: R01HL103866 and P01HL147823, S.L.H.); R01HL133169, R01HL148110, R01HL168493 and U54HL170326 (H.A.); Pilot Project Programs of the USC Center for Genetic Epidemiology and Southern California Environmental Health Sciences Center (P30ES007048) (J.A.H.); and the Deutsche Forschungsgemeinschaft (WI 5229/1-1) (M.W.). M.F. was supported, in part, by NIH training grants T32 HL134622 and T32 GM007250. A.H. is a participant in the BIH-Charité Advanced Clinician Scientist Program funded by Charité – Universitätsmedizin Berlin and the Berlin Institute of Health. The LipidCardio study (U.L. and I.D.) was partially supported by Sanofi-Aventis Deutschland GmbH. We also gratefully acknowledge the UK Biobank Resource for providing access to their data under application number 33307.

Author information

Marco Witkowski

Present address: Department of Cardiology, Angiology and Intensive Care, Deutsches Herzzentrum der Charité, Campus Benjamin Franklin, Berlin, Germany

Tomas Cajka

Present address: Institute of Physiology of the Czech Academy of Sciences, Prague, Czech Republic

Authors and Affiliations

Department of Cardiovascular & Metabolic Sciences, Lerner Research Institute, Cleveland Clinic, Cleveland, OH, USA

Marc Ferrell, Zeneng Wang, James T. Anderson, Xinmin S. Li, Marco Witkowski, Joseph A. DiDonato, Naseer Sangwan, W. H. Wilson Tang & Stanley L. Hazen

Systems Biology and Bioinformatics Program, Department of Nutrition, Case Western Reserve University, Cleveland, OH, USA

Marc Ferrell

Department of Population and Public Health Sciences, Keck School of Medicine, University of Southern California, Los Angeles, CA, USA

James R. Hilser, Jaana A. Hartiala & Hooman Allayee

Department of Biochemistry & Molecular Medicine, Keck School of Medicine, University of Southern California, Los Angeles, CA, USA

James R. Hilser & Hooman Allayee

Department of Cardiology, Angiology and Intensive Care, Deutsches Herzzentrum der Charité, Campus Benjamin Franklin, Berlin, Germany

Arash Haghikia & Ulf Landmesser

German Center for Cardiovascular Research (DZHK), Partner Site Berlin, Berlin, Germany

Arash Haghikia & Ulf Landmesser

Berlin Institute of Health (BIH), Berlin, Germany

Arash Haghikia & Ulf Landmesser

Friede Springer Cardiovascular Prevention Center at Charité, Berlin, Germany

Arash Haghikia & Ulf Landmesser

Charité – Universitätsmedizin Berlin, corporate member of Freie Universität Berlin and Humboldt-Universität zu Berlin, Berlin, Germany

Arash Haghikia & Ulf Landmesser

West Coast Metabolomics Center, University of California, Davis, Davis, CA, USA

Tomas Cajka & Oliver Fiehn

Department of Endocrinology and Metabolism, Charité – Universitätsmedizin Berlin, Berlin, Germany

Ilja Demuth, Maximilian König & Elisabeth Steinhagen-Thiessen

Berlin Institute of Health Center for Regenerative Therapies, Berlin, Germany

Ilja Demuth

Department of Cardiovascular Medicine, Heart, Vascular and Thoracic Institute, Cleveland Clinic, Cleveland, OH, USA

W. H. Wilson Tang & Stanley L. Hazen

Contributions

M.F. participated in the design, performance and analysis of all studies presented and drafted the manuscript, with input from all authors. All authors participated in the preparation of the manuscript. Z.W. and X.L. performed mass spectrometry analysis. J.A. performed chemical synthesis. O.F. and T.C. performed untargeted metabolomics data acquisition. J.R.H., J.A.H. and H.A. performed and assisted in genomic analyses. J.A.D. designed viral genomes. N.S. performed RNA sequencing analysis. A.H., M.W., I.D., M.K., E.S.-T., U.L. and W.H.W.T. provided valuable insights on clinical studies. S.L.H. conceived, supervised and participated in the design of all studies presented.

Corresponding author

Correspondence to [Stanley L. Hazen](#).

Ethics declarations

Competing interests

S.L.H. and Z.W. report being named as co-inventors on pending and issued patents held by the Cleveland Clinic relating to cardiovascular diagnostics and therapeutics. S.L.H. and Z.W. also report having received royalty payments for inventions or discoveries related to cardiovascular diagnostics or therapeutics from Cleveland Heart Lab, a fully owned subsidiary of Quest Diagnostics, and Procter & Gamble. S.L.H. is a paid consultant for Zehna Therapeutics and Procter & Gamble and has received research funds from Zehna Therapeutics, Procter & Gamble, Pfizer and Roche Diagnostics. W.H.W.T. is a consultant for Sequana Medical A.V., Cardiol Therapeutics, Genomics plc, Zehna Therapeutics and Renovacor and has received honoraria from Springer Nature for authorship/editorship and from the American Board of Internal Medicine for exam writing committee service. All other authors declare no competing interests.

Peer review

Peer review information

Nature Medicine thanks Matej Orešič and the other, anonymous, reviewer(s) for their contribution to the peer review of this work. Primary Handling Editor: Michael Basson, in collaboration with the *Nature Medicine* team.

Additional information

Publisher's note Springer Nature remains neutral with regard to jurisdictional claims in published maps and institutional affiliations.

Extended data

Extended Data Fig. 1 Network module-based pathway analysis identifies MACE-associated pathways containing MACE-associated metabolites.

(**center scatterplot**) MACE-associated metabolite enrichment scores versus enrichment P values for metabolic pathways (each point represents a pathway) defined in the Human MFN genome-scale metabolic model, as released with Metaboanalyst v4.0 ([Supplemental Methods](#)). Previously, Human MFN was constructed as a network by defining all human metabolites listed in KEGG (release 81.0), SMPDB v2.0, HMDB v4.0, ChEBI (release 131), and Biocyc (release 17.0) as points (nodes) and all chemical reactions (enzymatic or otherwise) as connections (edges) between metabolites ([Supplemental Methods](#)). Thus, any two molecules (nodes) participating in the same enzymatic reaction are connected with a line (edge). Metabolites (nodes) are separated into pathways (modules) to maximize the ratio of within-group to between-group connections. Pathway enrichment scores (ratio of observed to expected MACE-associated metabolites) and enrichment P values were determined with mummichog (v1.0.10), as implemented in Metaboanalyst v4.0 ([Supplemental Methods](#)), which includes adjustment for multiple testing. In the center scatterplot, each point represents the enrichment score (ratio of observed to expected MACE-associated metabolites) and the P value for the pathway (module). Each pathway (module) with enrichment P value < 0.05 and at least one component metabolite (node) with prospective 3-year MACE hazard ratio (highest vs lowest quartile) P < 0.005 is

highlighted in red. P values for all metabolites and pathways are shown in Supplemental Table 5. (**outer modules**) Shown are nine pathways (network modules) that were enriched with MACE-associated metabolites (enrichment P values < 0.05) and contained at least one component metabolite associated with prospective 3-year MACE (hazard ratio P < 0.005, two-sided Wald test assuming a univariate Cox model with no adjustment for multiple testing). Spectral features detected during untargeted metabolomics analysis were assigned to any molecule with a predicted mass-to-charge ratio within measurement error of the observed m/z , producing multiple assignments per feature ([Supplemental Methods](#)). Names of each network module-based pathway are shown, and within each pathway, lines (edges) indicate a shared metabolic conversion between the two connected metabolites (nodes), and metabolites (nodes) are colored according to the magnitude of the prospective 3-year MACE hazard ratio. Note that the “Vitamin B3 Metabolism” (niacin/NAD metabolism) pathway module was enriched with MACE-associated metabolites (enrichment P = 0.048) and the top unidentified metabolite (by incident MACE risk hazard ratio), with $m/z = 153.0656$ Da was assigned to both 2PY and 4PY within the “Vitamin B3 Metabolism” pathway module.

[Source data](#)

Extended Data Fig. 2 Overview of vitamin B3 metabolism, as defined in the Human MetaFishNet (MFN) model.

(a) Network module for vitamin B3 (niacin/NAD) metabolism. Previously, Human MFN was constructed as a network by defining all human metabolites listed in KEGG (release 81.0) SMPDB v2.0, HMDB v4.0, ChEBI (release 131) and Biocyc (release 17.0) as points (nodes) and all chemical reactions (enzymatic or otherwise) as connections (edges) between metabolites ([Supplemental Methods](#)). Thus, any two molecules (nodes) participating in the same enzymatic reaction are connected with a line (edge). Metabolites (nodes) are separated into pathways (modules) to maximize the ratio of within-group to between-group connections. Pathway enrichment P values (MACE cases vs controls) were determined with mummichog (v1.0.10), as implemented in Metaboanalyst v4.0 ([Supplemental Methods](#)), which includes adjustment for multiple

testing. The vitamin B3 network module was enriched with MACE-associated metabolites (enrichment $P = 0.048$), and a mass spectral feature ($m/z = 153.0656$ Da) assigned to metabolites (nodes) 2PY and 4PY was associated with prospective 3-year MACE risk (highest vs lowest quartile, unadjusted hazard ratio (HR) [95% confidence interval (CI)] = 2.77[1.59–4.86], $P = 0.005$ [two-sided Wald test, no adjusted for multiple testing]). Further CVD risk analysis of this mass spectral feature is shown in Fig. [2a-b](#). Metabolite (node) colors indicate the MACE hazard ratio (highest vs lowest quartile), while grey indicates the metabolite was not detected. Edges indicate a shared metabolic conversion between the two connected metabolites. Cofactors are not labeled. P values for all metabolites and pathways are shown in Supplemental Table [5](#). **(b)** Pathway representation of vitamin B3 metabolism using the molecules and reactions defined in the Human MFN model. The conversion of iminoaspartate to quinolinate was inferred in Human MFN, and so no enzyme is listed. NAD, nicotinamide adenine dinucleotide; ACMS, aminocarboxymuconate semialdehyde; NAMN, nicotinic acid mononucleotide; SAM Sadenosyl methionine; SAH, S-adenosyl homocysteine.

[Extended Data Fig. 3 Serum metabolite \(\$m/z = 153.0656\$ Da\) produces CID spectrum similar to a mixture of synthetic 2PY and 4PY.](#)

Untargeted metabolomics revealed a serum analyte ($m/z = 153.0656$ Da) associated with prospective residual MACE risk. Network module-based pathway analysis suggested this serum analyte ($m/z = 153.0656$ Da) was a mixture of the structural isomers 2PY and 4PY, which have the same elemental composition ([Supplemental Methods](#)). As the collision-induced dissociation (CID) mass spectrum of the MACE-associated serum analyte ($m/z = 153.0656$ Da) included characteristic daughter ions of both 2PY and 4PY, we explored whether a mixture of synthetic 2PY and 4PY could reproduce the CID mass spectrum of the serum analyte before conducting further structural studies and developing a method of independently quantitating 2PY and 4PY. Chemical synthesis of 2PY and 4PY is described in [Supplemental Methods](#), and $^1\text{H-NMR}$ spectra of synthetic material are shown in Supplemental Figs. [1](#) and [2](#). **(a)** Comparison of the high-resolution collision-induced dissociation (CID) mass spectra in positive ion mode of the unknown MACE-associated serum analyte with $m/z = 153.0656$ Da and calculated elemental formula

$C_7H_8O_2N_2$ (top), with synthetic 2PY (middle) and 4PY (bottom). 2PY and 4PY both have the elemental formula $C_7H_8O_2N_2$, and their observed m/z values are within measurement error (5 ppm) of 153.0656 Da. A CID parent-to-daughter transition characteristic, but not unique to 2PY ($m/z = 110.0605$ Da) is shown in red while a CID transition characteristic to 4PY ($m/z = 136.0395$ Da) is shown in blue. The spectrum of the serum analyte (top) contained parent-to-daughter transitions characteristic of 2PY and 4PY. **(b)** Parent-to-daughter transitions that are predicted to be unique to 2PY ($m/z = 126.0555$ Da) and 4PY ($m/z = 95.0133$ Da). These unique daughter fragments are detected at very low intensities as shown in Source Data. **(c)** We hypothesized the serum analyte with $m/z = 153.0656$ Da was a mixture of 2PY and 4PY. Without the capability to chromatographically separate 2PY and 4PY and compare to pure authentic chemical standards, we estimated the molar ratio of 2PY and 4PY in human serum in order to compare the presumed mixture to an equivalent mixture of 2PY and 4PY chemical standards. The molar ratio of 2PY:4PY in solution can be calibrated with the ratio of unique predicted parent-to-daughter transition intensities. The calibration curve prepared using 2PY and 4PY chemical standards in deionized water is shown. This molar ratio calibration curve was only used for exploratory structural studies and does not estimate absolute concentrations of 2PY and 4PY. Later, different calibration curves were used for independent quantitation of 2PY and 4PY using chromatographic separation. **(d)** Comparison of CID spectra of serum analyte with $m/z = 153.0656$ Da (top) with a solution of 2PY and 4PY in deionized water at the estimated molar ratio.

[Source data](#)

[Extended Data Fig. 4 Illustration of methods development to selectively monitor and quantify serum levels of 2PY and 4PY.](#)

Shown is the baseline chromatographic resolution of 2PY and 4PY in serum, coupled with the selective MRM transitions used to quantify 2PY and 4PY. Briefly, isotope labeled synthetic 2PY and 4PY (d3-2PY and d3-4PY) were added to serum samples, protein precipitated with methanol, and then following injection on silica column, the indicated isotopologues of 2PY and 4PY were resolved and monitored by the indicated MRM

transitions. The selectivity of the MRM transitions for either 2PY (red) or 4PY (blue) are indicated, with change in font size used to indicate selectivity for either 2PY or 4PY (or their corresponding d3-isotopologue internal standards). Chemical synthesis of 2PY and 4PY is described in [Supplemental Methods](#), and ¹H-NMR of synthetic material are shown in Supplemental Figs. [1](#) and [2](#). Note that the three distinct MRM transitions selected for monitoring natural abundance 2PY, 4PY, and their heavy isotope-labeled are also shown. The selected MRM transitions are also shown in Fig. [2d](#). Note how the silica column-based method baseline resolves 2PY and 4PY within the MACE-associated serum analyte with $m/z = 153.0656$ Da.

[Source data](#)

[Extended Data Fig. 5 Verifying the MACE-associated serum analyte with \$m/z = 153.0656\$ Da is comprised of 2PY and 4PY.](#)

The MACE-associated serum analyte with $m/z = 153.0656$ Da was resolved into two chromatographically separable structural isomers, 2PY and 4PY, using the new HPLC method. The two analytes have retention times of 2.4 min (metabolite 1; 2PY) and 3.4 min (metabolite 2; 4PY). **(a)** High resolution CID spectrum of serum metabolite 1 with retention time 2.4 min compared to synthetic 2PY (retention time 2.4 min). Peaks are labeled with their measured m/z in Da. **(b)** Sizes of predicted fragments of 2PY. Predicted fragments are labeled with their predicted m/z in Da. **(c)** CID spectrum of metabolite 2 with retention time 3.4 min compared to synthetic 4PY (retention time 3.4 min). Peaks are labeled with their measured m/z in Da. **(d)** Sizes of predicted fragments of 4PY. Predicted fragments are labeled with their predicted m/z in Da. Chemical synthesis of 2PY and 4PY is described in [Supplemental Methods](#), and ¹H-NMR spectra of synthetic material are shown in Supplemental Figs. [1](#) and [2](#). Differences in m/z among predicted fragments and those observed for synthetic and serum 2PY and 4PY were within expected experimental error and are shown in Supplemental Table [6](#).

[Source data](#)

Extended Data Fig. 6 Comparison of 2PY and 4PY levels in US and European Validation Cohorts.

(a - b) Serum levels of 2PY and 4PY were highly correlated in both the US and European Validation Cohorts. P values for Pearson correlations determined from t distributions with $n-2$ degrees of freedom ($P = 1.2 \times 10^{-1757}$ for the US validation cohort and $P = 2.1 \times 10^{-986}$ for the European validation cohort). P values for Spearman correlations determined with two-sided asymptotic t tests, and exact P values $< 2 \times 10^{-16}$ could not be determined. (c) Spearman correlations among 2PY, 4PY, and risk factors for MACE. P values determined with two-sided asymptotic t tests and adjusted for multiple testing using the false discovery rate method. Baseline clinical cohort characteristics are shown in Supplemental Table 2. ** $p < 0.0001$, * $p < 0.05$.

Extended Data Fig. 7 Sensitivity analysis of 2PY and 4PY association with MACE in the merged cohort.

US and European Validation Cohorts were merged ($n = 3,163$), and Hazard Ratio (quartile 4 (Q4) versus quartile 1 (Q1); open circle) for 4PY (panel a) and 2PY (panel b) association with MACE (3 yr) risks for the indicated subgroups are shown. Baseline clinical cohort characteristics are shown in Supplemental Table 2. Symbols represent hazard ratios and error bars represent 95% confidence intervals. Ref, reference group. Interaction P values were determined with two-sided Wald tests and adjusted for multiple testing using the method of Benjamani and Hochberg.

Source data

Extended Data Fig. 8 Transcriptomic analysis of human endothelial cells exposed to 2PY or 4PY.

(a) Human endothelial cells were cultured with 2PY, 4PY, or vehicle control, and RNA was harvested after 4 hours. *VCAM1* mRNA levels determined by RNA sequencing were elevated in 4PY-treated cells. The bar plot with error bars shows the mean plus or minus one standard error. P values were determined with two-sided Kruskal-Wallis (KW) and Wilcox tests. (b) Volcano plot shows differentially expressed genes for vehicle vs 4PY. (c) Differentially expressed genes for 2PY vs 4PY. Genes whose mRNA expression is

impacted by 4PY compared to either control are shown in red. Fold change P values were determined using the log ratio test as implemented in edgeR and adjusted using the false discovery rate method. **(d)** Gene sets (Gene Ontology terms) whose member genes are enriched with the differentially expressed genes between vehicle and 4PY are shown. Dot size indicates the number of differentially expressed genes in the set. P values determined with two sided Fisher Exact tests and adjusted using the false discovery rate method. Only tip terms are shown, that is enriched GO terms with enriched child terms are not shown. All enriched GO terms are included in Source Data. **(e)** Genes associated with the cellular response to tumor necrosis factor (TNF) (shown in red in **(d)**) tend to have higher expression in 4PY-treated cells than vehicle- and 2PY-treated cells. Expression in transcripts per million transformed to Z-scores per gene.

[Source data](#)

Extended Data Table 1 Meta-analysis results for lead variants associated with circulating 2PY, 4PY and sVCAM-1 levels

Extended Data Table 2 2PY, 4PY and sVCAM-1 levels across associated genome-wide significant variant (rs10496731) genotypes in the US validation cohort

Supplementary information

[Supplementary Information](#)

Supplementary Tables 1–8 and Supplementary Figs. 1–6.

[Reporting Summary](#)

Source data

[Source Data Fig. 1](#)

Statistical source data.

Source Data Fig. 2

Statistical source data.

Source Data Fig. 3

Statistical source data.

Source Data Fig. 4

Statistical source data.

Source Data Fig. 5

Statistical source data.

Source Data Fig. 5g

Uncropped intravital microscopy images of auricular venules of mice treated with 2PY, 4PY or vehicle control.

Source Data Extended Data Fig. 1

Statistical source data.

Source Data Extended Data Fig. 3

Statistical source data.

Source Data Extended Data Fig. 4

Statistical source data.

Source Data Extended Data Fig. 5

Statistical source data.

Source Data Extended Data Fig 7

Statistical source data.

Source Data Extended Data Fig 8

Statistical source data.

Rights and permissions

Springer Nature or its licensor (e.g. a society or other partner) holds exclusive rights to this article under a publishing agreement with the author(s) or other rightsholder(s); author self-archiving of the accepted manuscript version of this article is solely governed by the terms of such publishing agreement and applicable law.

[Reprints and permissions](#)

About this article

Cite this article

Ferrell, M., Wang, Z., Anderson, J.T. *et al.* A terminal metabolite of niacin promotes vascular inflammation and contributes to cardiovascular disease risk. *Nat Med* **30**, 424–434 (2024).

<https://doi.org/10.1038/s41591-023-02793-8>

Received

16 March 2023

Accepted

22 December 2023

Published

19 February 2024

Issue Date

February 2024

DOI

<https://doi.org/10.1038/s41591-023-02793-8>

Subjects

[Cardiovascular diseases](#)

• [Metabolomics](#)

• [Risk factors](#)

Nature Medicine (*Nat Med*) | ISSN 1546-170X (online) | ISSN 1078-8956 (print)